Journal of Sound and Vibration (2001) **248**(2), 235–246
doi:10.1006/jsvi.2001.3687, available online at http://www.idealibrary.com on IDEAL®

DETERMINATION OF THE RUBBING LOCATION IN A MULTI-DISK ROTOR SYSTEM BY MEANS OF DYNAMIC STIFFNESS IDENTIFICATION

F. Chu and W. Lu

Department of Precision Instruments, Tsinghua University, Beijing 100084, *People's Republic of China.*
E-mail: chufl@pim.tsinghua.edu.cn

(*Received* 18 *August* 2000, *and in final form* 17 *January* 2001)

The rotor-to-stator rub is one of the main serious malfunctions that often occur in rotating machinery. Previous research has provided enough tools to judge the existence of this fault. However, it is still a difficult task to detect the rubbing position in a multi-disk rotor system. In this paper, the stiffness is considered as variable and the rub-impact effect is included in this dynamic stiffness. Based on simulation data the least-square method is used to identify the dynamic stiffness at different positions along the rotor. It is found that the dynamic stiffness at the position where the rub-impact occurs is increasing as the rubbing develops and this stiffness at other positions shows very little change. The damping coefficients have similar trends. This method is found to be very effective in detecting the rubbing position.

1. INTRODUCTION

The rotor-to-stator rub is one of the main serious malfunctions that often occur in rotating machinery. It is usually a secondary phenomenon resulting from other faults, such as imbalance, misalignment, or fluid-induced, self-excited vibrations, which all result in high lateral vibration amplitudes and/or changes in the shaft centerline position within available clearances. When the rub happens, partial rub can be observed at first. During one complete period the rotor and stator have rubbing and impacting interaction once or fewer times. Gradual aggravation of the partial rub will lead to full rub and severe vibration makes normal operation of the machine impossible.

Rotor-to-stator rub in a rotating assembly has attracted great attention from researchers. There have been numerous publications on this topic. Muszynska's literature survey [1] gave a list of previous papers on the rub-related vibration phenomena. She discussed the physical meaning and the thermal effect of rub, various phenomena during rubbing, analysis and vibration response of rubbing rotors, and other related phenomena such as friction, impacting, stiffening and coupling effects. Beatty [2] suggested a mathematical model for rubbing forces which was non-linear with a piecewise linear form. The model is still considered as the most appropriate one to describe the rubbing effect. Through theoretical simulation and laboratory verification he concluded some useful points for diagnosing this fault. Choy and Padovan [3] performed a very interesting theoretical investigation to observe the effects of casing stiffness, friction coefficient, imbalance load and system damping on rub force history, and the transient response of rotor orbit. Muszynska [4] analyzed the physical phenomena related to partial lateral rotor-to-stator rub. By using

0022-460X/01/470235 + 12 $35.00/0

a periodic step function the analysis showed the existence of harmonic vibrations in the order 1/2, 1/3, 1/4, … ; experiment also confirmed the results. Other vibration characteristics of the rub-impact rotor system are also investigated, such as the influence of torsion on rotor/stator contact [5] and the bifurcation and chaotic phenomena [6].

Based on these research it is not so difficult to judge whether a rotor system has rubbing or not. For partial rub the vibration waveform of the shaft will have truncation. When the rub is developed into full rub, the rotor vibration shows backward orbiting, which is a special feature to identify the rotor-to-stator rub, distinguishing this malfunction from the others. However, it is still a difficult task to pinpoint the rubbing position.

Oks *et al.* [7] presented a method to detect the rubbing point in a rotor system by investigating the distribution of the amplitude of higher harmonics included in the response along the rotor. In this paper, another method is suggested using a rotor system with three disks. Since the rubbing has a strong stiffening effect, the dynamic stiffness at different positions is identified during the operation of the rotor system to examine the relation between this stiffness and the rubbing. The system is simplified as a three-mass system. When one of the disks is in contact with the stator, vibration signals are recorded. Then the system is considered as a mass-stiffness-damping system without including the rubbing effect, and the least-square method is used to identify the dynamic stiffness for three positions. By investigating the trend of the stiffness for different positions, the rubbing location can be found. This method is found to be very effective.

2. FORMULATION

In order to simulate the rubbing effect, we need to establish the equations of motion for the rub-impact system to produce the simulation data for identification purposes. The system discussed is a rotor system with three disks supported by ball bearings at two ends, as shown in Figure 1. The equivalent lumped masses at three disk positions are m_1, m_2 and m_3. The shaft sections between masses are considered as elastic and massless. The radial displacements at three disk positions are assumed as x_i, y_i $(i = 1, 2, 3)$. Imbalance at three disks is u_i $(i = 1, 2, 3)$. The differential equations of motion for this rub-impact rotor system can then be written as

$$\begin{bmatrix} m_1 & 0 & 0 \\ 0 & m_2 & 0 \\ 0 & 0 & m_3 \end{bmatrix} \begin{Bmatrix} \ddot{y}_1 \\ \ddot{y}_2 \\ \ddot{y}_3 \end{Bmatrix} + \begin{bmatrix} c_1 & 0 & 0 \\ 0 & c_2 & 0 \\ 0 & 0 & c_3 \end{bmatrix} \begin{Bmatrix} \dot{y}_1 \\ \dot{y}_2 \\ \dot{y}_3 \end{Bmatrix}$$

$$+ \begin{bmatrix} k_{11} & k_{12} & k_{13} \\ k_{21} & k_{22} & k_{23} \\ k_{31} & k_{32} & k_{33} \end{bmatrix} \begin{Bmatrix} y_1 \\ y_2 \\ y_3 \end{Bmatrix} = \begin{bmatrix} m_1 u_1 \omega^2 \sin(\omega t) + F_{y1} - m_1 g \\ m_2 u_2 \omega^2 \sin(\omega t) + F_{y2} - m_2 g \\ m_3 u_3 \omega^2 \sin(\omega t) + F_{y3} - m_3 g \end{bmatrix},$$

$$\begin{bmatrix} m_1 & 0 & 0 \\ 0 & m_2 & 0 \\ 0 & 0 & m_3 \end{bmatrix} \begin{Bmatrix} \ddot{x}_1 \\ \ddot{x}_2 \\ \ddot{x}_3 \end{Bmatrix} + \begin{bmatrix} c_1 & 0 & 0 \\ 0 & c_2 & 0 \\ 0 & 0 & c_3 \end{bmatrix} \begin{Bmatrix} \dot{x}_1 \\ \dot{x}_2 \\ \dot{x}_3 \end{Bmatrix}$$

$$+ \begin{bmatrix} k_{11} & k_{12} & k_{13} \\ k_{21} & k_{22} & k_{23} \\ k_{31} & k_{32} & k_{33} \end{bmatrix} \begin{Bmatrix} x_1 \\ x_2 \\ x_3 \end{Bmatrix} = \begin{bmatrix} m_1 u_1 \omega^2 \cos(\omega t) + F_{x1} \\ m_2 u_2 \omega^2 \cos(\omega t) + F_{x2} \\ m_3 u_3 \omega^2 \cos(\omega t) + F_{x3} \end{bmatrix}, \tag{1}$$

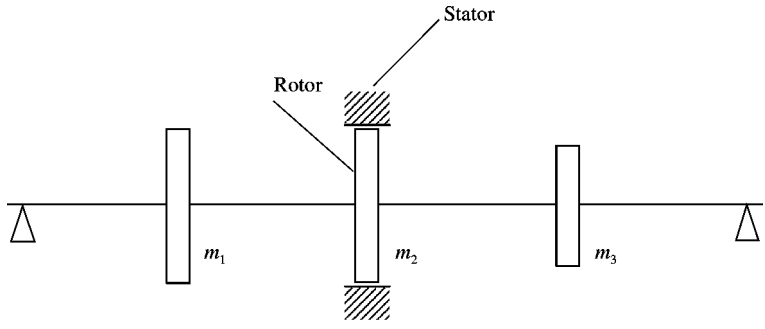

Figure 1. Schematic of a multi-disk rub-impact rotor system.

where c_i is the equivalent damping coefficient at the position of disk i, k_{ij} $(i = 1, 2, 3, j = 1, 2, 3)$ is the stiffness coefficient, this is, the necessary load value exerted at the position of the disk i in order to obtain a lateral deflection of unit at the position j and no lateral deflections at other positions, t is the time, F_x and F_y are the rub-impact force components in x and y directions, respectively, and the dot above the variables represents the derivative to time t.

It is assumed that there is an initial clearance of δ between rotor and stator. Compared with one complete period of rotating, the time during rub-impact is very short, therefore, an elastic impact model is used. Also, the Coulomb type of frictional relationship is assumed in the simulation. When rubbing happens, the radial impact force F_N and the tangential rub force F_T can thus be expressed [6] as

$$F_N(x, y) = \begin{cases} 0 & (\text{for } e < \delta) \\ (e - \delta)k_c & (\text{for } e \geqslant \delta) \end{cases} \quad F_T = fF_N,$$

where f is the friction coefficient between rotor and stator, k_c, is the radial stiffness of the stator and $e = \sqrt{x^2 + y^2}$ is the radial displacement of the rotor. These two forces can be written in x–y co-ordinates as

$$\begin{aligned} F_x(x, y) &= -F_N \cos\gamma + F_T \sin\gamma \\ F_y(x, y) &= -F_N \sin\gamma - F_T \cos\gamma \end{aligned} \quad \text{or} \quad \begin{Bmatrix} F_x \\ F_y \end{Bmatrix} = -\,\mathrm{H}(e - \delta)\frac{(e - \delta)k_c}{e}\begin{bmatrix} 1 & -f \\ f & 1 \end{bmatrix}\begin{Bmatrix} x \\ y \end{Bmatrix}, \tag{2}$$

where $\mathrm{H}: IR \to IR$ is the Heaviside function, that is,

$$\mathrm{H}(x) = \begin{cases} 0, & x \leqslant 0, \\ 1, & x > 0. \end{cases}$$

Equation (2) indicates that when the rotor displacement e is smaller than δ, the static clearance between rotor and stator, there will be no rub-impact interaction and the rub-impact forces are zero while the rub-impacting will happen if the rotor displacement e is bigger than δ.

The fourth order Runge–Kutta method is used to integrate equation (1) to obtain data with rub-impact effect. During the calculation a smaller integration step has to be chosen to ensure a stable solution and to avoid the numerical divergence at the point where derivatives of F_x and F_y are discontinuous. Generally long time-marching computation is needed to obtain a convergent orbit. After discarding the transients, steady state data are obtained for further identification purposes. Parameters used in the computation are:

lumped masses $m_1 = 3{\cdot}5$ kg, $m_2 = 4{\cdot}0$ kg, $m_3 = 3{\cdot}0$ kg; damping coefficients $c_{11} = 1{\cdot}05 \times 10^3$ N s/m, $c_{22} = 1{\cdot}2 \times 10^3$ N s/m, $c_{33} = 0{\cdot}9 \times 10^3$ N s/m; stiffness coefficients $k_{11} = 3{\cdot}1543 \times 10^7$ N/m, $k_{22} = 4{\cdot}3885 \times 10^7$ N/m, $k_{33} = 3{\cdot}1543 \times 10^7$ N/m, $k_{12} = k_{21} = -3{\cdot}0173 \times 10^7$ N/m, $k_{13} = k_{31} = 1{\cdot}2342 \times 10^7$ N/m, $k_{23} = k_{32} = -3{\cdot}0173 \times 10^7$ N/m; the stiffness coefficient of the stator $k_c = 0{\cdot}5 \times 10^9$ N/m; the static clearance between rotor and stator $\delta = 0{\cdot}1 \times 10^{-3}$ m; the friction coefficient $f = 0{\cdot}2$.

We will now consider the rotor system as a three-mass system without the rotor-to-stator interaction by assuming that the stiffness at three positions is variable and the rub-impact effect is ignored. The variable stiffness can be considered as dynamic stiffness and the rub-impact effect is reflected by this dynamic stiffness. Equation (1) can thus be transferred into

$$\begin{bmatrix} m_1 & 0 & 0 \\ 0 & m_2 & 0 \\ 0 & 0 & m_3 \end{bmatrix} \begin{Bmatrix} \ddot{y}_1 \\ \ddot{y}_2 \\ \ddot{y}_3 \end{Bmatrix} + \begin{bmatrix} c_1 & 0 & 0 \\ 0 & c_2 & 0 \\ 0 & 0 & c_3 \end{bmatrix} \begin{Bmatrix} \dot{y}_1 \\ \dot{y}_2 \\ \dot{y}_3 \end{Bmatrix} + \begin{bmatrix} k_{11} & k_{12} & k_{13} \\ k_{21} & k_{22} & k_{23} \\ k_{31} & k_{32} & k_{33} \end{bmatrix} \begin{Bmatrix} y_1 \\ y_2 \\ y_3 \end{Bmatrix} = \begin{bmatrix} m_1 u_1 \omega^2 \sin(\omega t) - m_1 g \\ m_2 u_2 \omega^2 \sin(\omega t) - m_2 g \\ m_3 u_3 \omega^2 \sin(\omega t) - m_3 g \end{bmatrix}$$

$$\begin{bmatrix} m_1 & 0 & 0 \\ 0 & m_2 & 0 \\ 0 & 0 & m_3 \end{bmatrix} \begin{Bmatrix} \ddot{x}_1 \\ \ddot{x}_2 \\ \ddot{x}_3 \end{Bmatrix} + \begin{bmatrix} c_1 & 0 & 0 \\ 0 & c_2 & 0 \\ 0 & 0 & c_3 \end{bmatrix} \begin{Bmatrix} \dot{x}_1 \\ \dot{x}_2 \\ \dot{x}_3 \end{Bmatrix} + \begin{bmatrix} k_{11} & k_{12} & k_{13} \\ k_{21} & k_{22} & k_{23} \\ k_{31} & k_{32} & k_{33} \end{bmatrix} \begin{Bmatrix} x_1 \\ x_2 \\ x_3 \end{Bmatrix} = \begin{bmatrix} m_1 u_1 \omega^2 \cos(\omega t) \\ m_2 u_2 \omega^2 \cos(\omega t) \\ m_3 u_3 \omega^2 \cos(\omega t) \end{bmatrix}, \tag{3}$$

where k and c are variables to be identified.

In order to simplify the identification process, we have made some assumptions. The stiffening action caused by the rotor-to-stator rub will generally have the strongest effect at the position where the rubbing occurs. Therefore, we only identify k_{11}, k_{22} and k_{33} with the assumption of other k's unchanged. We will see later that these three stiffness coefficients will be enough to show the relation between the dynamic stiffness and the rotor-to-stator interaction.

Equation (3) can be rewritten as

$$\begin{cases} c_1 \dot{x}_1 + k_{11} x_1 = m_1 u_1 \omega^2 \cos(\omega t) - k_{12} x_2 - k_{13} x_3 - m_1 \ddot{x}_1, \\ c_1 \dot{y}_1 + k_{11} y_1 = m_1 u_1 \omega^2 \sin(\omega t) - k_{12} y_2 - k_{13} y_3 - m_1 \ddot{y}_1 - m_1 g, \end{cases} \tag{4}$$

$$\begin{cases} c_2 \dot{x}_2 + k_{22} x_2 = m_2 u_2 \omega^2 \cos(\omega t) - k_{21} x_1 - k_{23} x_3 - m_2 \ddot{x}_2, \\ c_2 \dot{y}_2 + k_{22} y_2 = m_2 u_2 \omega^2 \sin(\omega t) - k_{21} y_1 - k_{23} y_3 - m_2 \ddot{y}_2 - m_2 g, \end{cases} \tag{5}$$

$$\begin{cases} c_3 \dot{x}_3 + k_{33} x_3 = m_3 u_3 \omega^2 \cos(\omega t) - k_{31} x_1 - k_{32} x_2 - m_3 \ddot{x}_3, \\ c_3 \dot{y}_3 + k_{33} y_3 = m_3 u_3 \omega^2 \sin(\omega t) - k_{31} y_1 - k_{32} y_2 - m_3 \ddot{y}_3 - m_3 g. \end{cases} \tag{6}$$

The following form of solutions for x_i and y_i can be assumed:

$$\begin{aligned} x_i &= a_{i0x} + a_{i1x}\cos\omega t + b_{i1x}\sin\omega t + a_{i2x}\cos 2\omega t + b_{i2x}\sin 2\omega t + \cdots \\ y_i &= a_{i0y} + a_{i1y}\cos\omega t + b_{i1y}\sin\omega t + a_{i2y}\cos 2\omega t + b_{i2y}\sin 2\omega t + \cdots \end{aligned} \qquad i = 1, 2, 3. \tag{7}$$

Differentiating x_i and y_i gives

$$\begin{aligned} \dot{x}_i &= -a_{i1x}\omega\sin\omega t + b_{i1x}\omega\cos\omega t - 2a_{i2x}\omega\sin 2\omega t + 2b_{i2x}\omega\cos 2\omega t + \cdots \\ \dot{y}_i &= -a_{i1y}\omega\sin\omega t + b_{i1y}\omega\cos\omega t - 2a_{i2y}\omega\sin 2\omega t + 2b_{i2y}\omega\cos 2\omega t + \cdots \end{aligned} \qquad i = 1, 2, 3, \tag{8}$$

$$\begin{aligned} \ddot{x}_i &= -a_{i1x}\omega^2\cos\omega t - b_{i1x}\omega^2\sin\omega t - 4a_{i2x}\omega^2\cos 2\omega t - 4b_{i2x}\omega^2\sin 2\omega t + \cdots \\ \ddot{y}_i &= -a_{i1y}\omega^2\cos\omega t - b_{i1y}\omega^2\sin\omega t - 4a_{i2y}\omega^2\cos 2\omega t - 4b_{i2y}\omega^2\sin 2\omega t + \cdots \end{aligned} \qquad i = 1, 2, 3. \tag{9}$$

By substituting equations (7), (8), and (9) into, say, equation (4) and equating the coefficients for $\cos\omega t$, $\sin\omega t$, $\cos 2\omega t$, $\sin 2\omega t, \ldots$ on the two sides, the following equation can then be obtained:

$$As = b, \tag{10}$$

where

$$[A] = \begin{bmatrix} A_1 \\ A_2 \end{bmatrix}, \quad \{b\} = \begin{Bmatrix} b_1 \\ b_2 \end{Bmatrix}, \quad \{s\} = [c_1, k_{11}]^{\mathrm{T}}, \quad [A_1] = \begin{bmatrix} \omega b_{11x} & a_{11x} \\ -\omega a_{11x} & b_{11x} \\ 2\omega b_{12x} & a_{12x} \\ -2\omega a_{12x} & b_{12x} \\ \vdots & \vdots \end{bmatrix},$$

$$[A_2] = \begin{bmatrix} \omega b_{11y} & a_{11y} \\ -\omega a_{11y} & b_{11y} \\ 2\omega b_{12y} & a_{12y} \\ -2\omega a_{12y} & b_{12y} \\ \vdots & \vdots \end{bmatrix},$$

$$\{b_1\} = \begin{bmatrix} m_1u_1\omega^2 - k_{12}a_{21x} - k_{13}a_{31x} + m_1\omega^2 a_{11x} \\ -k_{12}b_{21x} - k_{13}b_{31x} + m_1\omega^2 b_{11x} \\ -k_{12}a_{22x} - k_{13}a_{32x} + 4m_1\omega^2 a_{12x} \\ -k_{12}b_{22x} - k_{13}b_{32x} + 4m_1\omega^2 b_{12x} \\ \vdots \end{bmatrix},$$

$$\{b_2\} = \begin{bmatrix} m_1u_1\omega^2 - k_{12}a_{21y} - k_{13}a_{31y} + m_1\omega^2 a_{11y} \\ -k_{12}b_{21y} - k_{13}b_{31y} + m_1\omega^2 b_{11y} \\ -k_{12}a_{22y} - k_{13}a_{32y} + 4m_1\omega^2 a_{12y} \\ -k_{12}b_{22y} - k_{13}b_{32y} + 4m_1\omega^2 b_{12y} \\ \vdots \end{bmatrix}.$$

The row number of the matrix A_1 or A_2 depends on the series selected in equation (7). In the following calculation we have kept the series terms to $\cos 8\omega t$ and $\sin 8\omega t$. The elements in matrices A and b can be obtained by the Fourier transform of the simulated steady state time-domain responses. Therefore, the undetermined coefficients s can be calculated by the least-square method through

$$s = (A^{\mathrm{T}}A)^{-1}A^{\mathrm{T}}b. \tag{11}$$

The dynamic stiffness and damping at other two positions can be identified by the same way as k_{11} and c_1 by substituting equations (7), (8), and (9) into equations (4) and (5) respectively.

3. RESULTS AND DISCUSSION

For a practical rotor system, the lumped masses can be determined through some ways. Also, the value and position of the imbalance can be obtained by, for example, the method

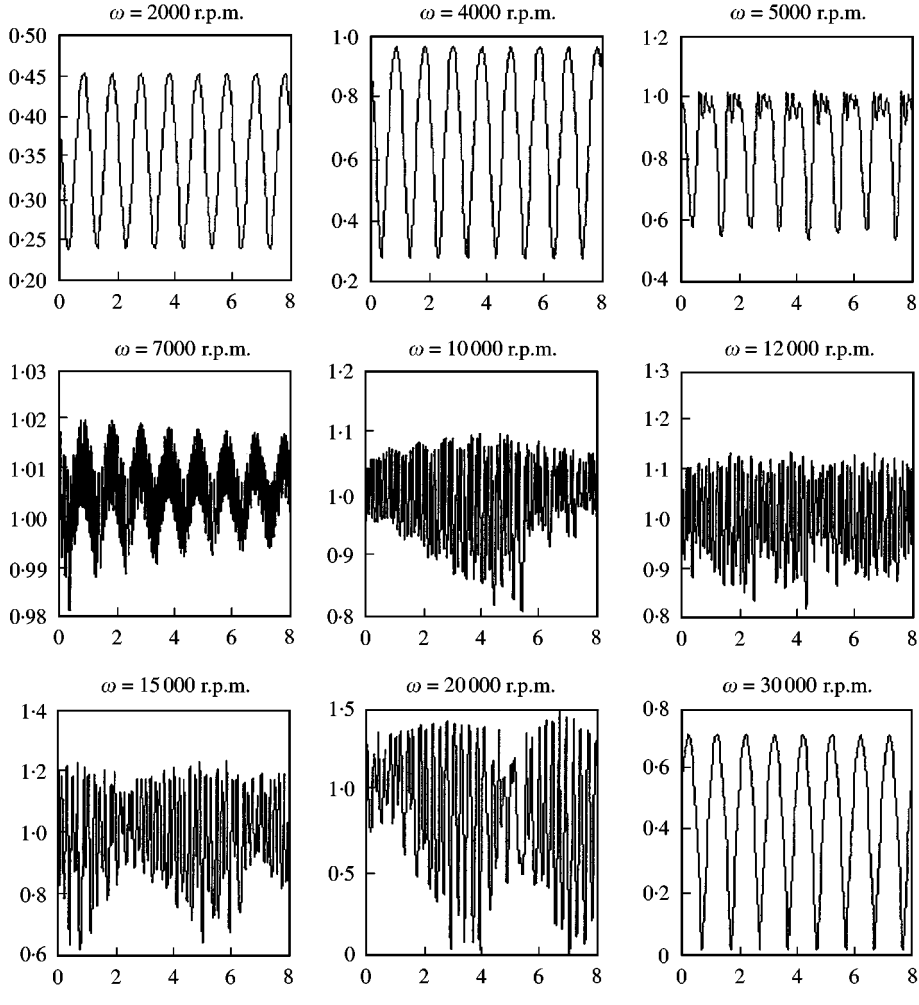

Figure 2. The vibration waveforms of $\sqrt{x_2^2 + y_2^2}$ at different rotating speeds (abscissas are in number of rotations and ordinates are in $\sqrt{x_2^2 + y_2^2}/\delta$).

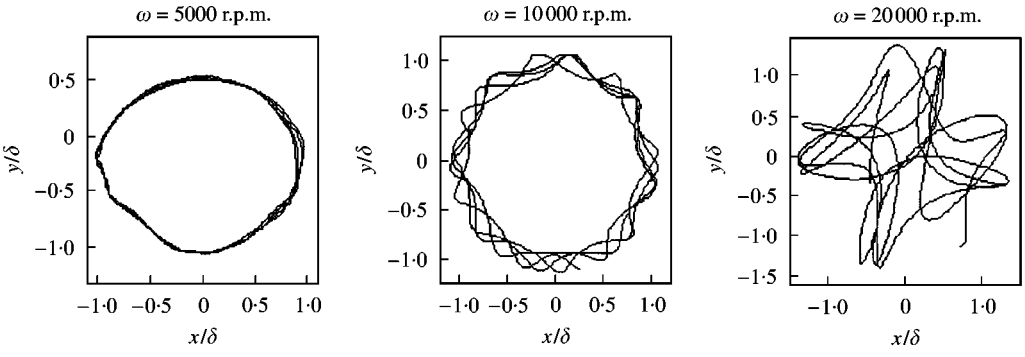

Figure 3. Vibration orbits at the middle disk position.

introduced in reference [8]. Therefore, during the identification process mass m and imbalance u are considered as known parameters. In the following identification calculation, parameter values of m given in the last section are used.

We now assume that $u_1 = 0$, $u_2 = 0{\cdot}13$ mm, $u_3 = 0$, and the rotor and stator interact at the position of m_2. In the following, we use the fourth order Runge–Kutta method to integrate equation (1) at first to obtain vibration data at three positions for every rotating speed. Based on these simulation data and equation (3) the least-square method is then used to identify stiffness and damping coefficients as discussed in the last section.

The rotating speed is increased to observe the identification process. At low rotating speeds, vibration is not so obvious and the rub-impact does not occur, as shown in Figure 2 for $\omega = 2000$ and 4000 r.p.m., in the waveform of the radial displacement ($\sqrt{x^2 + y^2}$) at the position of m_2. At about $\omega = 5000$ r.p.m., partial rub begins to occur. The truncation of the waveform can be observed. After this rotating speed, the rub-impact effect becomes more severe as the rotating speed is increased. We have calculated these simulation data until $\omega = 20\,000$ r.p.m. At $\omega = 30\,000$ r.p.m., the rubbing effect has ceased and the vibration waveform resumes its normal state. In Figure 3 some typical orbits at the middle disk position are given. The first figure shows just the beginning of the rubbing. At $\omega = 10\,000$ and 20 000 r.p.m., the rotor-to-stator interaction appears more and more severe and the motion has some chaotic feature. We have also given some vibration waveforms and orbits at the position of m_1 for comparison, as shown in Figure 4. It can be seen that at $\omega = 5000$ r.p.m., the vibration curve and the orbit have similar forms to those at the middle disk position (in Figures 2 and 3). This has confirmed that from the vibration curve and the orbit, one can diagnose the existence of the rotor-to-stator interaction and cannot find the position of this interaction.

Based on these data, equation (3) is then used to identify stiffness and damping coefficients. The identification results are shown in Figures 5 and 6. From Figure 5 it can be seen that when the partial rub happens, k_{22} has a slight increase, and as the rub-impact becomes severe, k_{22} keeps increasing. At $\omega = 30\,000$ r.p.m., because the rub-impact has stopped, this dynamic stiffness has resumed the value as that for no rotor-to-stator interaction. For other positions, although the rub-impact is developing, k_{11} and k_{33} have very little change. Therefore, the trend of the dynamic stiffness can be an indication for the rub-impact interaction and can be used to detect the position where the rub-impact happens. Figure 6 is the identification results for the damping coefficients where the same trend can be observed.

We now see another case where $u_1 = 0$, $u_2 = 0{\cdot}15$ mm, $u_3 = 0$, and the rotor and stator interact at the position of m_1. Figure 7 gives the vibration waveforms at the position of m_1

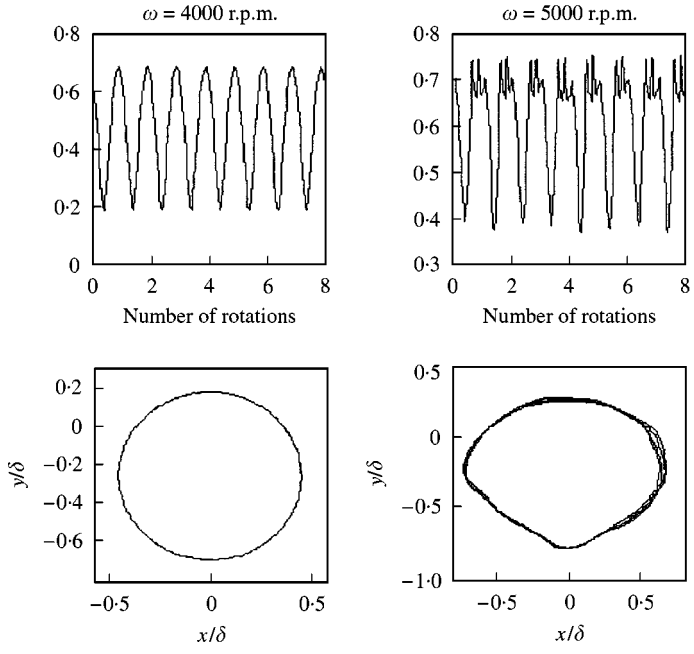

Figure 4. The vibration waveforms and orbits at the position of m_1.

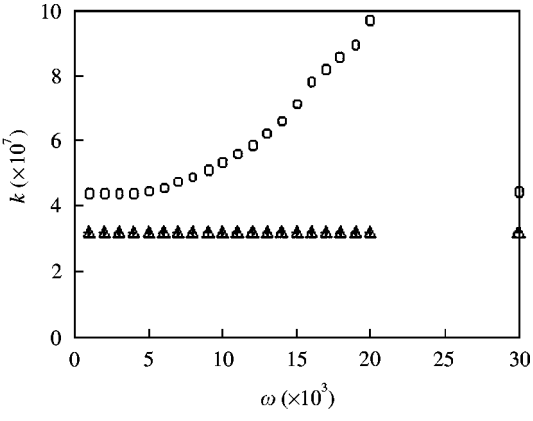

Figure 5. The dynamic stiffness obtained by the least-square identification (ω in rpm and k in N/m). *, k_{11}; O, k_{22}; Δ, k_{33}.

for different rotating speeds. At $\omega = 5000$ r.p.m., partial rub can be seen from the figure. When $\omega = 7000$ through 8000 to 9000 r.p.m., severe rub-impact can be observed. At $\omega = 11\,000$ r.p.m., vibration becomes normal again without the rub-impact effect. Figures 8 and 9 show the identification results. It can again be seen that at the position of the rub-impact interaction, the dynamic stiffness will be increasing as the rub-impact develops, and at other positions the dynamic stiffness has very little change. The dynamic damping shows a similar trend. It can also be found that when the rubbing stops, the dynamic stiffness and damping will immediately drop to their original values.

The third example is shown in Figure 10 where the rub-impact rotor system has five disks. The disks can be numbered as m_1 to m_5 from the left. The parameters used in this

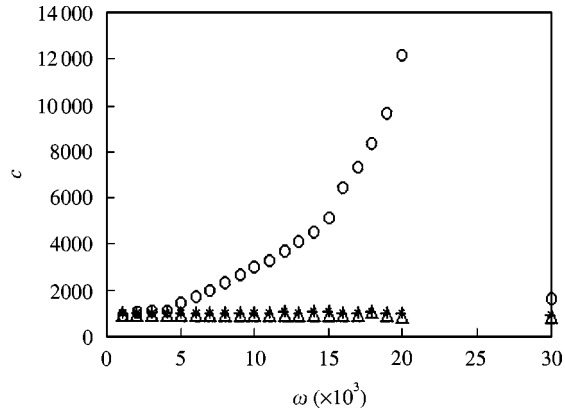

Figure 6. Damping coefficients obtained by the least-square identification (ω in rpm and c in N s/m). $*$, c_1; O, c_2; Δ, c_3.

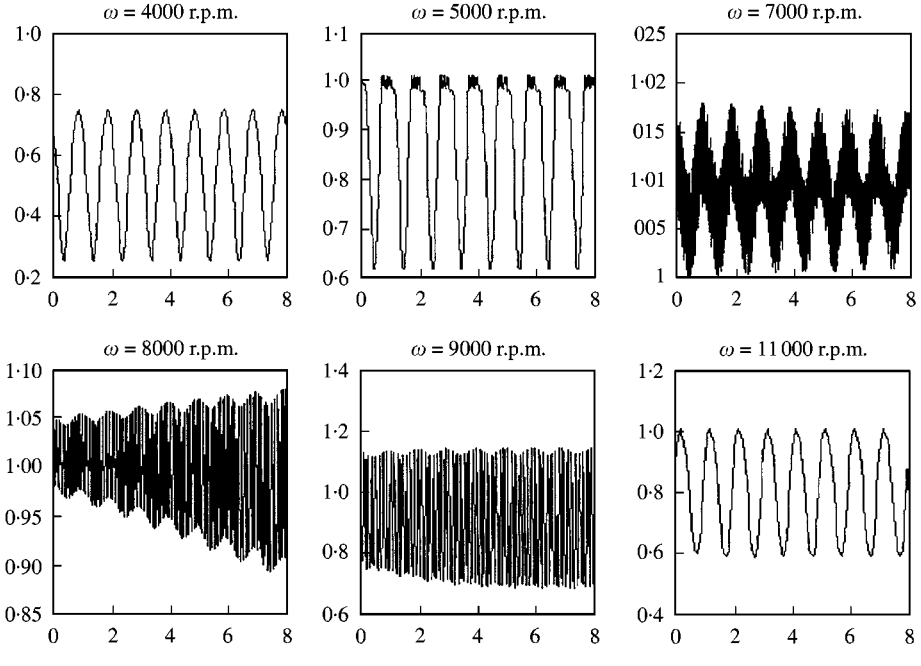

Figure 7. The vibration waveforms of $\sqrt{x_1^2 + y_1^2}$ at different rotating speeds (abscissas are in number of rotations and ordinates are in $\sqrt{x_1^2 + y_1^2}/\delta$).

example are: lumped masses $m_1 = 1{\cdot}5$ kg, $m_2 = 2{\cdot}0$ kg, $m_3 = 2{\cdot}0$ kg, $m_4 = 1{\cdot}3$ kg, $m_5 = 1{\cdot}5$ kg; damping coefficients $c_{ii} = 300 \times m_{ii}$ N s/m ($i = 1, 2, 3, 4, 5$); stiffness coefficients $k_{11} = k_{55} = 0{\cdot}6972 \times 10^8$ N/m, $k_{22} = k_{44} = 2{\cdot}9186 \times 10^8$ N/m, $k_{33} = 5{\cdot}7 \times 10^8$ N/m, $k_{12} = k_{21} = -0{\cdot}998 \times 10^8$ N/m, $k_{13} = k_{31} = 0{\cdot}675 \times 10^8$ N/m, $k_{14} = k_{41} = -0{\cdot}1457 \times 10^8$ N/m, $k_{15} = k_{51} = 0{\cdot}0153 \times 10^8$ N/m, $k_{23} = k_{32} = -3{\cdot}4125 \times 10^8$ N/m, $k_{24} = k_{42} = 1{\cdot}3845 \times 10^8$ N/m, $k_{25} = k_{52} = -0{\cdot}1457 \times 10^8$ N/m, $k_{34} = k_{43} = -3{\cdot}4125 \times 10^8$ N/m, $k_{35} = k_{53} = 0{\cdot}675 \times 10^8$ N/m, $k_{45} = k_{54} = -0{\cdot}998 \times 10^8$ N/m; the stiffness coefficient of the stator $k_c = 0{\cdot}5 \times 10^{11}$ N/m; the static clearance between rotor and stator $\delta = 0{\cdot}3 \times 10^{-4}$ m;

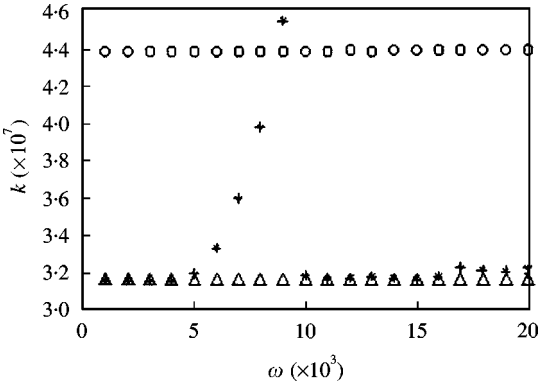

Figure 8. The dynamic stiffness obtained by the least-square identification (ω in rpm and k in N/m). ∗, k_{11}; ○, k_{22}; △, k_{33}.

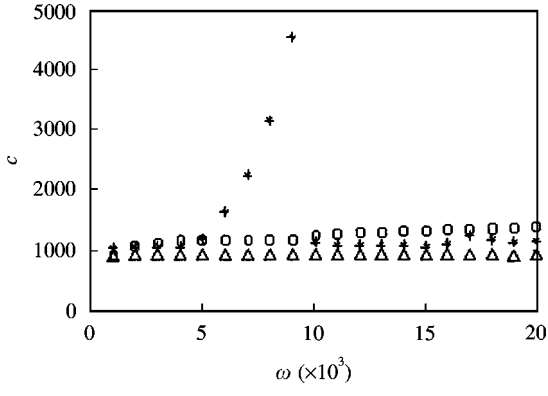

Figure 9. Damping coefficients obtained by the least-square identification (ω in rpm and c in N s/m). ∗, c_1; ○, c_2; △, c_3.

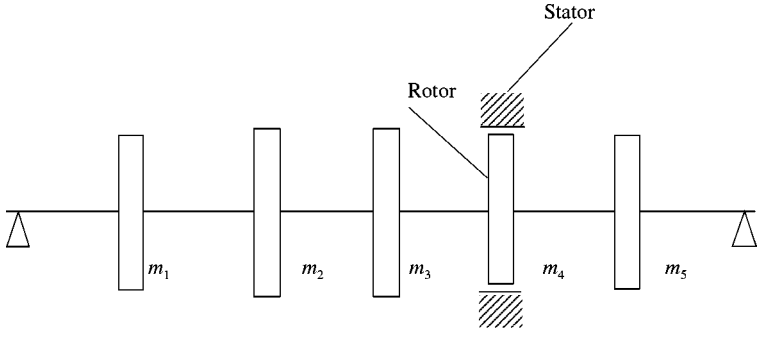

Figure 10. Schematic of the rub-impact rotor system with five disks.

and the friction coefficient $f = 0{\cdot}2$. We now assume that $u_1 = 0$, $u_2 = 0$, $u_3 = 0{\cdot}1$ mm, $u_4 = 0$, $u_5 = 0$, and the rotor and stator interact at the position of m_4. Eight terms are again assumed in the Fourier series of the responses and the identification results are shown in Figures 11 and 12. It can again be seen from the figures that the dynamic stiffness at the

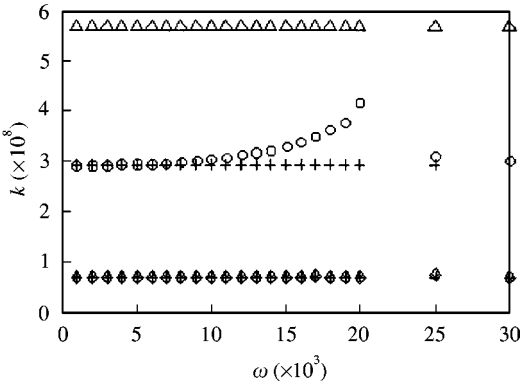

Figure 11. The dynamic stiffness obtained by the least-square identification (ω in rpm and k in N/m). $*$, k_{11}; $+$, k_{22}; Δ, k_{33}; $\bigcirc$, k_{44}; $\diamond$, k_{55}.

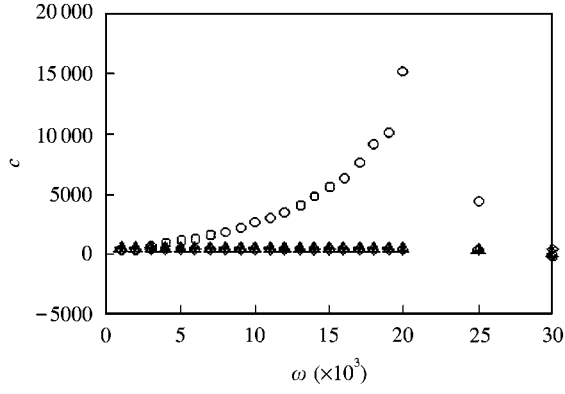

Figure 12. Damping coefficients obtained by the least-square identification (ω in rpm and c in N s/m). $*$, c_{11}; $+$, c_{22}; Δ, c_{33}; $\bigcirc$, c_{44}; $\diamond$, c_{55}.

position where the rotor-to-stator rub occurs has a clear increasing as the rubbing develops and this stiffness at other locations shows very little change. A similar trend can also be found in the identification results of the damping coefficients.

We have tried another case by increasing the imbalance to simulate the engineering rotor systems as in engineering applications imbalance will generally increase during the operation of the machine. The same results can still be observed.

4. CONCLUSIONS

Much research work has been done to diagnose the rub-impact fault in rotating machinery. For a multi-disk rotor system, there are some special features to find this fault, such as the truncation of the vibration waveform and the backward orbiting. A dynamic stiffness-based method is presented in this paper to detect the rubbing position.

It is shown from the analysis that the dynamic stiffness at the position where the rotor-to-stator rub occurs clearly increases as the rubbing develops. The stiffness at other positions shows very little change. The damping coefficients have similar trends. This idea can be used to detect the rubbing position effectively in a multi-disk rotor system. Based on

this method the data obtained from the condition monitoring system installed in important rotating machinery can be used to determine the rubbing location whenever the rotor-to-stator rub occurs. However, this method can only detect the position where the response of vibration can be measured.

ACKNOWLEDGMENTS

This research is financially supported by a project from the Ministry of Science and Technology of China (Grant Number PD9521908Z2) and National Natural Science Foundation of China (Grant No. 19990510).

REFERENCES

1. A. MUSZYNSKA 1989 *The Shock and Vibration Digest* **21**, 3–11. Rotor-to-stationary element rub-related vibration phenomena in rotating machinery—literature survey.
2. R. F. BEATTY 1985 *Transactions of the American Society of Mechanical Engineers, Journal of Vibration, Acoustics, Stress, and Reliability in Design* **107**, 151–160. Differentiating rotor response due to radial rubbing.
3. F. K. CHOY and J. PADOVAN 1987 *Journal of Sound and Vibration* **113**, 529–545. Non-linear transient analysis of rotor-casing rub events.
4. A. MUSZYNSKA 1984 *Proceedings of the 3rd International Conference on Vibration in Rotating Machinery, Institution of Mechanical Engineers, York, UK*, 327–335. Partial lateral rotor to stator rubs.
5. S. EDWARDS, A. W. LEES and M. I. FRISWELL 1999 *Journal of Sound and Vibration* **225**, 767–778. The influence of torsion on rotor/stator contact in rotating machinery.
6. F. CHU and Z. ZHANG 1998 *Journal of Sound and Vibration* **210**, 1–18. Bifurcation and chaos in a rub-impact Jeffcott rotor system.
7. A. B. OKS, T. IWATSUBO and S. ARII 1993 *JSME International Journal Series C* **36**(3), 312–318. Detection of the point where rubbing occurs in a multisupported rotor system.
8. J. M. KRODKIEWSK, J. DING and N. ZHANG 1994 *Journal of Sound and Vibration* **169**, 685–698. Identification of unbalance change using a nonlinear mathematical model for multi-bearing rotor systems.